Magnetic properties of the weak itinerant-electron ferromagnet $Ni_{75}Al_{25}$: II. The effect of compositional disorder

2004 J. Phys.: Condens. Matter 16 8695

(http://iopscience.iop.org/0953-8984/16/47/020)

INSTITUTE OF PHYSICS PUBLISHING JOURNAL OF PHYSICS: CONDENSED MATTER

J. Phys.: Condens. Matter **16** (2004) 8695–8712 PII: S0953-8984(04)75102-4

Magnetic properties of the weak itinerant-electron ferromagnet $Ni_{75}Al_{25}$: II. The effect of compositional disorder

S N Kaul[1] **and Anita Semwal**

School of Physics, University of Hyderabad, Central University PO, Hyderabad–500 046, Andhra Pradesh, India

E-mail: kaulsp@uohyd.ernet.in

Received 19 January 2004, in final form 21 May 2004
Published 12 November 2004
Online at stacks.iop.org/JPhysCM/16/8695
doi:10.1088/0953-8984/16/47/020

Abstract

The results of a detailed study of the magnetic properties of *well-characterized* polycrystalline Ni_pAl_{100-p} (73.5 at.% $\leqslant p \leqslant$ 76 at.%) alloys are presented and discussed in the light of the existing theories. Extreme care has been exercised in the sample preparation to ensure that the site disorder (invariably present in any alloy system) does not interfere with the compositional disorder brought about by the reduction in the concentration of the magnetic (Ni) atoms. Thus, the observed variation in the magnetic properties with Ni concentration (p) is solely controlled by the compositional disorder. Like site disorder, compositional disorder smears out the sharp features in the density of states (DOS) curve near the Fermi level, E_F, and reduces the DOS at E_F, $N(E_F)$, and thereby causes a fall (an enhancement) in the values (value) of the spontaneous magnetization at 0 K, M_0, the spin-wave stiffness at 0 K, D_0, and the Curie temperature, T_C (zero-field differential susceptibility at 0 K, χ_0). However, compositional disorder, unlike site disorder, gives rise to *smooth variations* in $N(E_F)$, the inverse Stoner enhancement factor $\mathcal{S}^{-1} = IN(E_F) - 1$, M_0, D_0, T_C, D_0/T_C and χ_0 with p. These variations in the case of $M_0(p)$, $D_0(p)$ and $T_C(p)$ are very well described by the power laws $M_0(p) \sim (p - p_c)^{\beta_p}$, $D_0(p) \sim (p - p_c)^{\theta_p}$ and $T_C(p) \sim (p - p_c)^{\phi}$ with $p > p_c$ (p_c = the percolation threshold for the appearance of long-range ferromagnetic order) predicted by the percolation theories for these quantities on a regular three-dimensional ($d = 3$) percolating network. The alloys in question exhibit a crossover in the spin dynamics from the hydrodynamic (*magnon*) to critical (*fracton*) regime at a well-defined temperature $T^*_{co}(p)$. An elaborate analysis of the magnetization data in terms of the percolation models permits a reasonably accurate determination of the magnon-to-fracton crossover line

[1] Author to whom any correspondence should be addressed.

in the magnetic phase diagram, the percolation-to-thermal crossover exponent, fractal dimension, fracton dimensionality, the percolation critical exponents for spontaneous magnetization, spin-wave stiffness, correlation length and conductivity. The results of this analysis also vindicate the Alexander–Orbach conjecture and the Golden inequality for $d = 3$ percolating ferromagnetic networks.

1. Introduction

According to the phase diagram [1] of binary Ni_pAl_{100-p} alloys, the intermetallic compound $Ni_{75}Al_{25}$ has a homogeneity range which extends from $p_l = 73.5$ at.% to $p_u = 76.5$ at.%. The investigations [2–9] of magnetic properties in the composition range $p_l \leqslant p \leqslant p_u$ have revealed that these properties are *extremely sensitive* to Ni concentration (p)—so much so that the long-range weak itinerant-electron ferromagnetism *breaks down completely* (i.e., the Curie temperature, T_C, *drops* to *zero*) if p *falls below* $p_c \approx 74.5$ at.% [2–7] and paves the way to exchange-enhanced paramagnetism for p just below p_c. By contrast, one such investigation due to Dhar *et al* [8] places this critical Ni concentration (p_c) at 75.1 ± 0.2 at.%. Even among those determinations [2–7] that are in good agreement as far as the value of p_c is concerned, widely different values of T_C for a given composition are observed. For instance, T_C varies from 25 K [4] to 43 K [7] for the stoichiometric composition. Dhar *et al* [8] observe that if the Ni concentrations of their samples are systematically shifted to *lower values* by ~0.6 at.%, their T_C values match the previously determined [2–7] ones. On the basis of this observation and the argument that, to some extent, Al is lost by evaporation during high-temperature annealing, these authors suggest that the nominal compositions reported [2–7] earlier are lower in Ni concentration by ~0.6 at.%. Subsequently, a detailed study [9] of magnetic and transport properties of chemically analysed Ni_pAl_{100-p} alloys yielded values of T_C that conform well with those reported in [6, 7], based on nominal compositions. At this stage, it should be noted that in view of the inferences drawn in the preceding paper [10] (henceforth referred to as paper I) regarding the role of site disorder, the wide dispersion in the T_C values for a given composition could *partly* result from the fact that the samples of nearly the same composition, used in different investigations, have been subjected to different heat treatments and hence are in different states of site disorder.

Magnetic properties of binary Ni_pAl_{100-p} alloys in the composition range $p_l \leqslant p \leqslant p_u$ but for $p \geqslant p_c$ have been interpreted in terms of either the Stoner–Wohlfarth (SWO) model [11, 12] or the self-consistent renormalization (SCR) theory of *non-propagating* spin fluctuations [13], as elucidated below. On the one hand, the result that the expressions $M(T, 0) = M(0, 0) - aT^2$ and $T_C(p) \sim (p - p_c)^{1/2}$, predicted by the SWO model, reproduce quite well respectively the observed temperature dependence of spontaneous magnetization, $M(T, 0)$, for $0.1T_C \leqslant T \leqslant 0.75T_C$ and the Ni concentration dependence of T_C for $p \geqslant p_c$ has been taken to imply [2, 3, 5] that the SWO model, which holds the Stoner single-particle spin-flip excitations solely responsible for the thermal demagnetization of $M(T, 0)$, adequately describes magnetism in the Ni_pAl_{100-p} alloys for $p_c \leqslant p \leqslant p_u$. On the other hand, on the basis of the observations that, in the temperature ranges $0.1T_C \leqslant T \leqslant 0.4T_C$ and $0.42T_C \leqslant T \leqslant T_C$, respectively, $M(T, 0)$ follows the relations $M^2(T, 0) = M^2(0, 0) - bT^2$ and $M^2(T, 0) = c(T_C^{4/3} - T^{4/3})$, predicted by the SCR spin fluctuation (SF) model, and that the variations of T_C and $M(0, 0)$ with Ni concentration, $T_C(p) \sim (p - p_c)^{1/2}$ and $M(0, 0) \sim (p - p_c)^{1/2}$, are also consistent with the predictions of this model, Sasakura *et al* [6] and Suzuki and Masuda [7] assert that the SCR-SF model, but not the SWO model, forms a

Table 1. Actual Ni and Al concentrations, lattice parameter, a, atomic long-range order parameter, **S**, magnetic moment per Ni atom at 5 K, μ_{Ni}, coefficient of the $\sqrt{H}$ term, η', and high-field susceptibility at 0 K, $\chi_{hf}(0)$.

Sample	Ni conc. (at.%)	Al conc. (at.%)	a (Å)	**S**	μ_{Ni} (μ_B)	η' ($\times 10^{-2}$ $Oe^{1/2}$)	$\chi_{hf}(0)$ ($\times 10^{-5}$)
S_{74}	74.31(9)	25.69(5)	3.5708(12)	0.76(4)	0.035(1)	5.3(3)	11.6(1)
S_{75}	74.73(9)	25.27(5)	3.5686(14)	0.77(4)	0.060(1)	4.2(4)	11.1(3)
S_{76}	75.98(8)	24.02(5)	3.5618(10)	0.76(2)	0.134(1)	2.5(3)	9.7(3)

correct description of magnetism in the alloys in question. The above observations concerning the temperature dependence of $M(T, 0)$ are, however, in direct contradiction with the *direct* (*indirect*) evidence for well-defined spin-wave excitations in $Ni_{75}Al_{25}$ at low temperatures from small-angle neutron scattering [14] and inelastic neutron scattering [15] experiments (recent high-precision magnetization data [10, 16]).

From the foregoing critical assessment of the results reported so far, it is evident that a complete understanding of magnetism in the Ni_pAl_{100-p} alloys for $p_c \leqslant p \leqslant p_u$ is still lacking. Taking cognizance of the fact that the previous investigations [2–9] were plagued by the complex interplay between site disorder and compositional disorder and that they completely ignored the contribution due to spin-wave excitations, which are primarily responsible for the thermal demagnetization of $M(T, 0)$ and $M(T, H)$ at low temperatures [10, 16], we undertook a detailed magnetization study of Ni_pAl_{100-p} alloys in the Ni concentration range 74 at.% $\leqslant p \leqslant$ 76 at.%. The samples of different composition, used for magnetic measurements, were prepared under *identical* conditions without subjecting them to any annealing treatment. This strategy was deliberately adopted so as to ensure that all the samples had essentially the same *background* site disorder. The compositional dependence of the magnetic properties is thus solely controlled by the *additional* site disorder brought about by the variation in composition, i.e., by the *compositional disorder alone*.

2. Experimental details

Starting from 99.998% pure Ni and Al, polycrystalline rods, 100 mm in length and 10 mm in diameter, of the alloys with nominal composition $Ni_{74}Al_{26}$, $Ni_{74.5}Al_{25.5}$, $Ni_{75}Al_{25}$ and $Ni_{76}Al_{24}$ were prepared by a radio-frequency (RF) induction technique following a procedure detailed elsewhere [17]. In an attempt to partly compensate for the loss of Al by evaporation during melting, a small amount of Al *in excess of* that suggested by the nominal composition was deliberately added to the alloy constituents before melting. Spheres of 2.5 mm diameter and discs of 10 mm diameter and 5 mm thickness were spark-cut from the alloy rods. A number of pieces cut from the different parts of the rod of given composition were analysed for chemical composition using the x-ray fluorescence technique and inductively coupled plasma optical emission spectroscopy. The actual chemical composition of the alloys is given in table 1. Consistent with the purity of the starting materials, the total concentration of magnetic 3d transition metal impurities such as Mn, Cr, Fe and Co was below 0.002 at.%. X-ray diffraction patterns were recorded for disc-shaped samples at room temperature over the angle, 2θ, range of $10^\circ \leqslant 2\theta \leqslant 100^\circ$, using Cu K$\alpha$ radiation. The observed x-ray patterns, shown in figure 1, could be completely indexed on the basis of the $L1_2$ cubic structure. Drastically *reduced* peak intensity and very *broad* Bragg peaks for the samples S_{74} and S_{75} (for sample labels, see the following text) compared to that for the sample S_{76} are manifestations of a fairly large

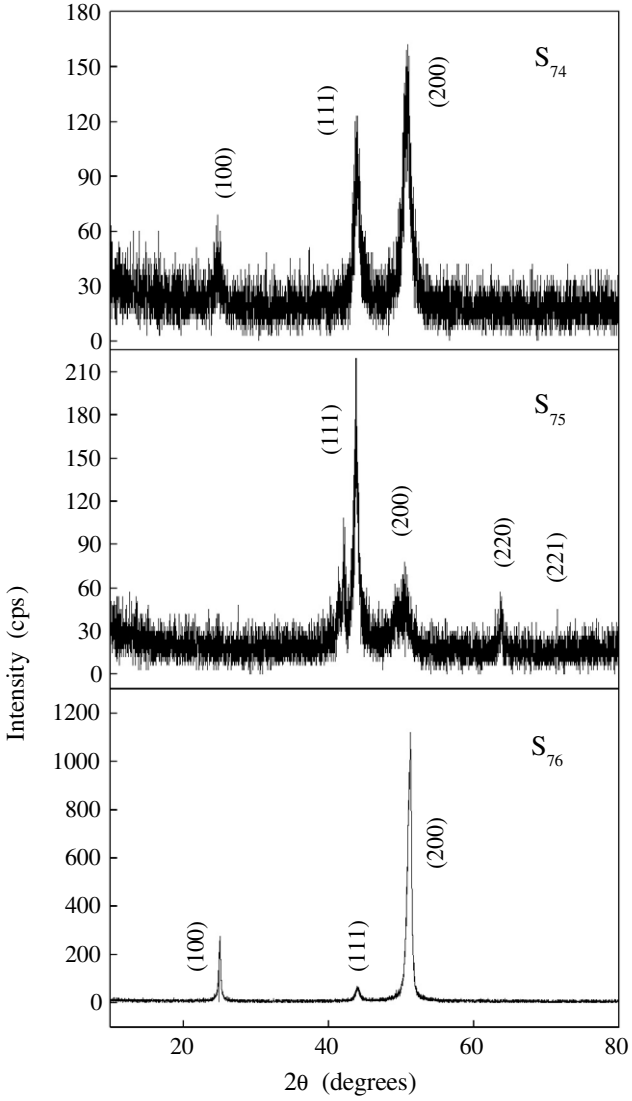

Figure 1. X-ray diffraction patterns at room temperature.

internal strain and/or *compositional inhomogeneity* in the former two samples. The refined values of the lattice parameter, a, and the numerical estimates for the atomic long-range order parameter, **S**, yielded by the elaborate analyses [17] of the x-ray diffraction data, are displayed in table 1. That, regardless of the Ni concentration, the alloys in question are roughly in the same site-disordered state is supported by the result that the long-range order parameter hardly varies with the Ni concentration (table 1). In view of the calculation of the site occupation of Ni and Al sublattices from the observed values of **S**, described in detail in section 3 of paper I, very low concentrations of impurities and vacancies (point defects) in the samples in question are not expected to have any significant influence on the site occupation and hence on the type of site disorder present; the site disorder in these samples mainly results from the antisite concentration of Ni and Al atoms.

Table 2. The Curie temperature, T_C, spin-wave stiffness at 0 K, D_0, the D_0/T_C ratio, magnon-to-fracton crossover temperature, T^*_{co}, and crossover frequency, ω_{co}.

Sample	T_C (K)	D_0 (meV Å^2)	D_0/T_C (meV Å^2 K^{-1})	T^*_{co} (K)	ω_{co} (10^{11} Hz)
S_{74}	47.60(5)	16(2)	0.34(4)	0.30(15)	0.4(2)
S_{75}	56.24(5)	32(2)	0.57(4)	4.90(75)	6.4(10)
S_{76}	76.30(5)	96.7(3)	1.267(5)	48.20(75)	63.0(10)

The magnetization (M) of polycrystalline Ni_pAl_{100-p} ($p = 73.52$, 74.31, 74.73 and 75.98) alloys with composition near the critical Ni concentration ($p_c = 74.5$) was measured as a function of the external magnetic field (H_{ext}) at a temperature $T = 5$ K in fields up to 70 kOe and as a function of temperature at $H_{ext} = 1$ kOe in the temperature range $5\text{ K} \leqslant T \sim 2T_C$ (T_C = Curie temperature) with a relative accuracy of better than 10 ppm using a SQUID magnetometer. These measurements revealed that all the alloys, with the exception of the alloy with $p = 73.52$ (which is paramagnetic at temperatures down to 5 K), exhibit long-range ferromagnetic order at temperatures below T_C. The Curie temperature T_C for a given composition was determined from the Arrott ($M^2(T, H)$ versus $H/M(T, H)$, where $H = H_{ext} - 4\pi NM(T, H_{ext})$ and N is the demagnetizing factor [10]) plot, as detailed in paper I. These Arrott plots were constructed out of the $M(T, H_{ext})$ isotherms taken at different temperatures in fields up to 15 kOe using a vibrating sample magnetometer (VSM). The values of T_C so determined are displayed in table 2. Now as the main aim of this paper is to ascertain the effect of compositional disorder on the magnetic quantities of interest such as the spontaneous magnetization at 0 K, $M_0 \equiv M(0, 0)$, the spin-wave stiffness at 0 K, D_0, zero-field differential susceptibility at 0 K, $\chi_0 \equiv \chi(0, 0)$, density of states at the Fermi level, $N(E_F)$, and T_C, only the magnetization data for the alloys with $p = 74.31$, 74.73 and 75.98 (henceforth referred to as the samples S_{74}, S_{75} and S_{76}) are presented here. Note that Al atoms in Ni_pAl_{100-p} alloys do not possess any magnetic moment and hence act to produce magnetic dilution.

3. Data analysis, results and discussion

A complete loss of long-range ferromagnetic order at a critical value of the Ni concentration (the percolation threshold) suggests that the percolation ideas may have some relevance to the magnetism in the Ni_pAl_{100-p} alloys, even though these alloys are supposed to be weak itinerant-electron ferromagnets. Before ascertaining whether or not the effect of compositional disorder can be understood in terms of the percolation theories, an attempt has been made to analyse the magnetization data taken for the samples S_{74}, S_{75} and S_{76} in the same way as was done for the $Ni_{75}Al_{25}$ samples with varying degree of site disorder in paper I.

The spontaneous magnetization at 0 K for each concentration was obtained by fitting the $M(T = 5\text{ K}, H)$ isotherms for fields *above* the *technical saturation* to the expression $M(H) = M_0 + \eta'\sqrt{H} + \chi_{hf}H$ (equation (1) of paper I), where M_0 is the spontaneous magnetization at 5 K. The best least-squares fits (continuous curves) to the $M(T = 5\text{ K}, H)$ data (symbols), based on the above expression, are shown in figure 2 while the corresponding values of the parameters μ_{Ni} (magnetic moment per Ni atom, deduced from M_0), η' and the high-field susceptibility, χ_{hf}, are listed in table 1. The reduction in the parameter η' (which is a direct measure of the suppression of spin waves by the magnetic field) as p increases (table 1) can be qualitatively understood as follows. Since μ_{Ni} increases with p (table 1), the corresponding increase in the internal field results in the progressive suppression of spin

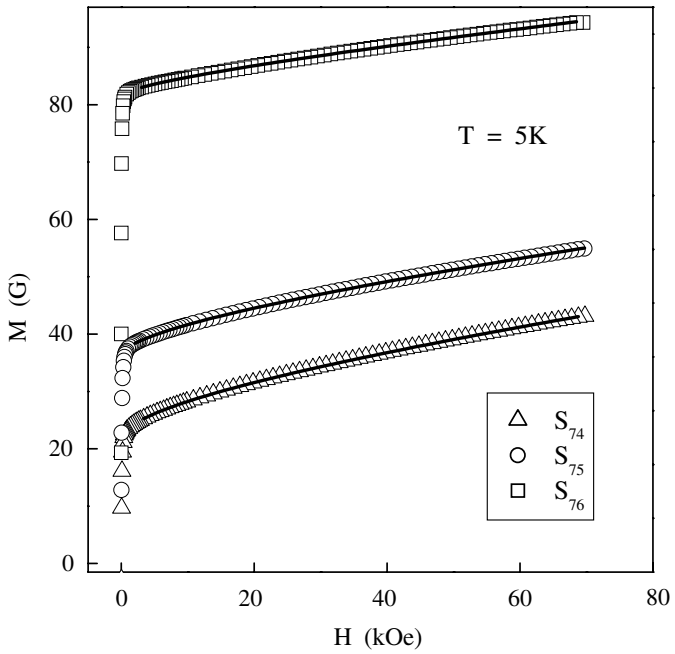

Figure 2. $M(H)$ isotherms at $T = 5$ K. The continuous curves through the data points (symbols) represent the best least-squares fits based on the expression given in the text.

waves—so much so that these low-lying magnetic excitations become less and less sensitive to the external magnetic field as p increases. Moreover, as both μ_{Ni} and χ_{hf} are related to the density of states (DOS) per atom per spin at the Fermi level, $N(E_{\mathrm{F}})$, through the equations (9) and (8) of paper I, the decline in η' and χ_{hf} as p increases (table 1) basically reflects a sizable enhancement in $N(E_{\mathrm{F}})$ with increasing Ni concentration.

M_0 and χ_0 (zero-field differential susceptibility at 0 K) have also been determined [10] from the Arrott ($[M(T, H)]^2$ versus $H/M(T, H)$) plots, constructed out of the $M(T = 5\,\mathrm{K}, H)$ data of figure 2 and displayed in figure 3. A close scrutiny of the data presented in figure 3 reveals a slight concave-downward (concave-upward) curvature in the Arrott plot isotherm (isotherms) for the sample (samples) S_{76} (S_{74} and S_{75}); the concave upward curvature becomes more pronounced as the Ni concentration decreases from 74.73 at.% in S_{75} to 74.31 at.% in S_{74}. Nevertheless, at high fields, the Arrott plot isotherms for all the three samples are roughly linear and a linear extrapolation in this field regime (which is much narrower than that for the samples used in paper I) was made to obtain reliable values for M_0 and χ_0. As observed in paper I, the M_0 values obtained by the above two methods are in excellent agreement with one another. χ_0 and the lattice parameter a are plotted against Ni concentration p in figure 4. The *linear* decrease in a with increasing p conforms very well with the variation of a with p reported [18] earlier in *ordered* $\mathrm{Ni}_p\mathrm{Al}_{100-p}$ alloys. The finding that the functional form of $a(p)$ is the *same* for site-disordered and ordered $\mathrm{Ni}_p\mathrm{Al}_{100-p}$ alloys re-emphasizes the conclusion drawn in paper I that the site disorder has practically no effect on the lattice parameter. This result also asserts that the observed variation of a with p is solely governed by the compositional disorder.

In sharp contrast with the magnetic behaviour observed [10] in site-disordered $\mathrm{Ni}_{75}\mathrm{Al}_{25}$ samples, the thermal demagnetization of $M(T, 0)$ and $M(T, H)$ for $T \leqslant T_{\mathrm{C}}$ in the samples

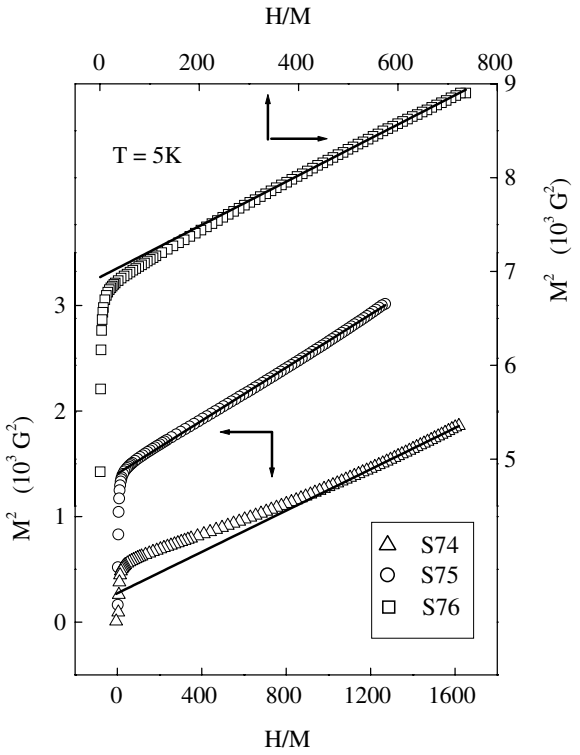

Figure 3. Arrott (M^2 versus H/M) plots constructed out of the $M(H)$ isotherms taken at $T = 5$ K and shown in figure 2. The solid straight lines through the data points (symbols) serve to illustrate the linear extrapolation to $H = 0$ used to obtain the spontaneous magnetization at 0 K, M_0.

under consideration does not follow the predictions (equations (3)–(6) of paper I) of any of the theoretical models [11–13, 19, 20] proposed for weak itinerant-electron ferromagnets. To elucidate this point further, attempts to fit equations (3)–(6) of paper I to the $M(T, 0)$ and $M(T, H)$ data over any reasonable temperature range for $T \leqslant T_C$ did not succeed. Next, the numerical estimates for the density of states (DOS) per atom per spin at the Fermi level, $N(E_F)$, were obtained by inserting the values of χ_0 determined here and the previously reported [21] value $I = 0.85$ eV of the Stoner parameter into the relation $N(E_F) = \chi_0/[I\chi_0 - N\mu_B^2]$ (which is an alternative form of equations (8) and (10) of paper I). The $N(E_F)$ values, so obtained, and the above value of the Stoner parameter I, when used in the expression $\mathcal{S}^{-1} = [IN(E_F) - 1]$, yield the values for the inverse Stoner enhancement parameter $\mathcal{S}^{-1}$ for different compositions. The variations of $N(E_F)$ and $\mathcal{S}^{-1}$ with Ni concentration p are shown in figure 5. Considering that the long-range ferromagnetic order is sustained only when $IN(E_F) > 1$ (the *Stoner criterion*), a theoretical fit to the $\mathcal{S}^{-1}(p)$ data has been attempted on the basis of the empirical relation $\mathcal{S}^{-1}(p) = A(p - p_c)^n$ so as to determine the *critical* Ni concentration (p_c) for the onset of long-range ferromagnetic order, at which $\mathcal{S}^{-1}(p_c) = 0$. The continuous curve through the $\mathcal{S}^{-1}(p)$ data, shown in figure 5, depicts the best (least-squares) fit based on the above relation with the parameter values $A = 0.0048(7)$, $p_c = 73.6(1)$ at.% Ni and $n = 1.30(1)$. Note that in arriving at the best fit, p_c is kept *fixed* at a certain value in the range $73 \leqslant p_c \leqslant 75$ (in steps of 0.01) while the other two parameters A and n are varied. In order to ascertain whether or not the reduction in $N(E_F)$ with decreasing (increasing) Ni concentration (compositional

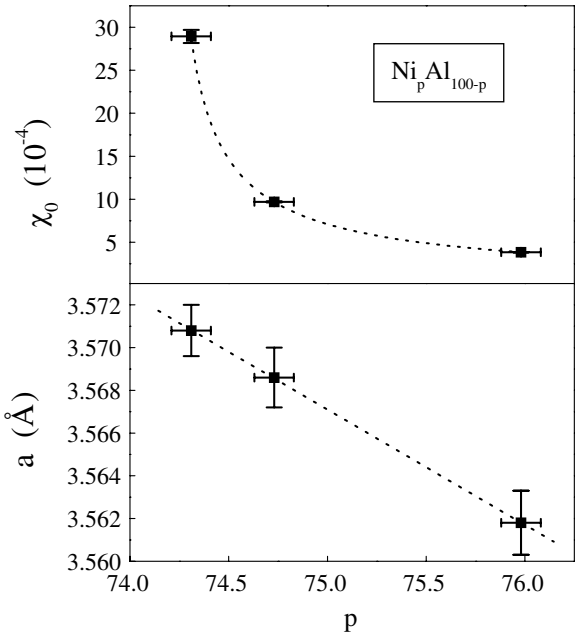

Figure 4. Variations of the lattice parameter a and the zero-field differential susceptibility at 0 K, χ_0, with the Ni concentration, p.

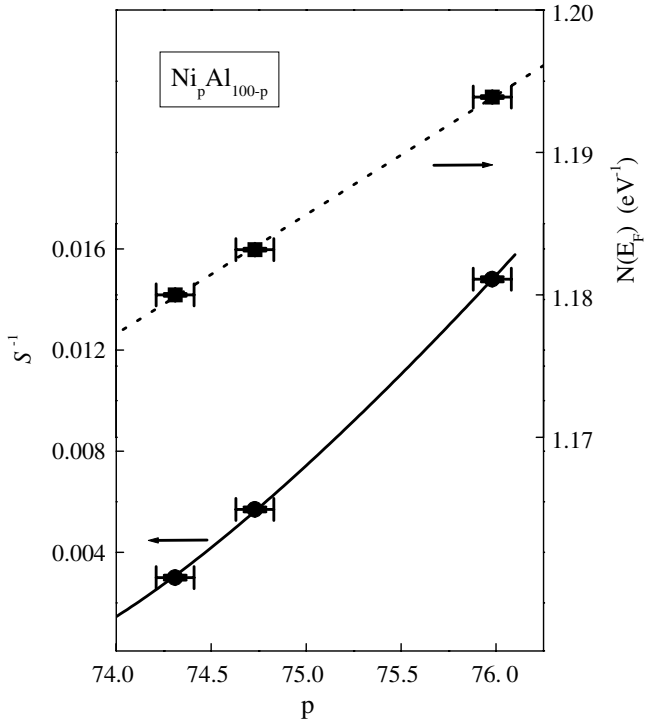

Figure 5. Variations of the inverse Stoner enhancement factor, $\mathcal{S}^{-1}$, and the density of states at the Fermi level, $N(E_F)$, with Ni concentration, p. Note that the error bars on $N(E_F)$ and $\mathcal{S}^{-1}$ are smaller than the size of the data symbols.

disorder) is associated with the change in the shape of the DOS curve near the Fermi level, E_F, caused by compositional disorder, we proceed along the same lines as in paper I and plot M_0 against $[N(E_F)]^2$ $(\mathcal{S}^{-1})^{1/2}$ (equation (14) of paper I) in figure 6 and T_C versus $M_0^{3/2}$

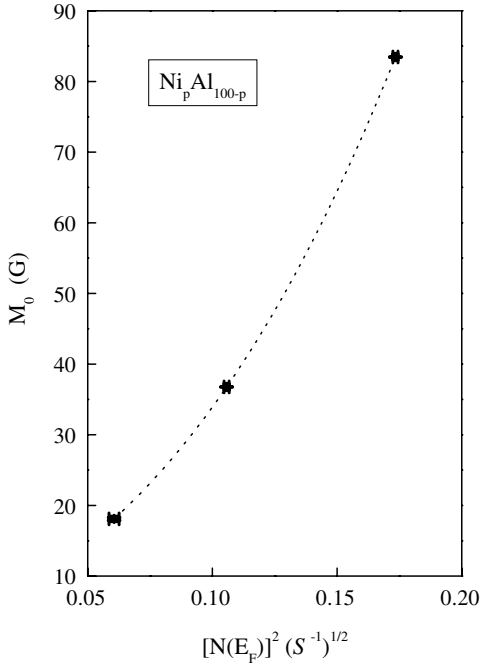

Figure 6. The spontaneous magnetization at 0 K, M_0, plotted against the quantity $[N(E_F)]^2$ $(S^{-1})^{1/2}$ (see the text).

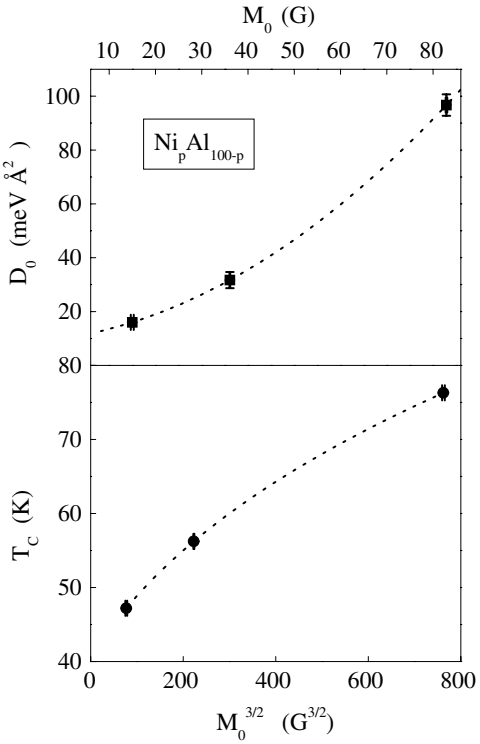

Figure 7. The D_0 versus M_0 and T_C versus $M_0^{3/2}$ plots.

(equation (17) of paper I) in figure 7. The *nonlinear* variations observed in figures 6 and 7 imply that the compositional disorder does change the shape of the DOS curve near E_F, in addition to reducing $N(E_F)$.

In the event that spin waves are the main cause for the thermal demagnetization at low temperatures (as was the case for the $Ni_{75}Al_{25}$ samples in paper I), a plot of the 'in-field' magnetization versus $T^{3/2}$ should exhibit a concave-downward curvature due to: (i) the presence of higher-order terms in the magnon dispersion relation; (ii) the temperature renormalization of the spin-wave stiffness; and (iii) the gap in the spin-wave spectrum introduced by magnetic field H and other anisotropy fields. In sharp contrast to this, a noticeable concave-upward curvature is observed in the M versus $T^{3/2}$ curves (figure 8), irrespective of the alloy composition. As the concentration of the magnetic (Ni) atoms approaches the *critical* value p_c from the higher side, this curvature becomes more and more prominent. This deviation from the expected behaviour is a strong indication for a *crossover* in the spin dynamics on a three-dimensional ferromagnetic *percolating* network from a *hydrodynamic* (magnon) regime at low temperatures to a *critical* (fracton) regime at high temperatures. Before ascertaining whether or not this is the case from an elaborate analysis of the $M(T, H)$ data, an attempt was made to find out whether the percolation theories [22–24] correctly describe the observed variations of M_0 and T_C with p.

For randomly diluted magnetic systems, the percolation theories [22–24] predict that the spontaneous magnetization (or the percolation probability) at 0 K, M_0, and Curie temperature,

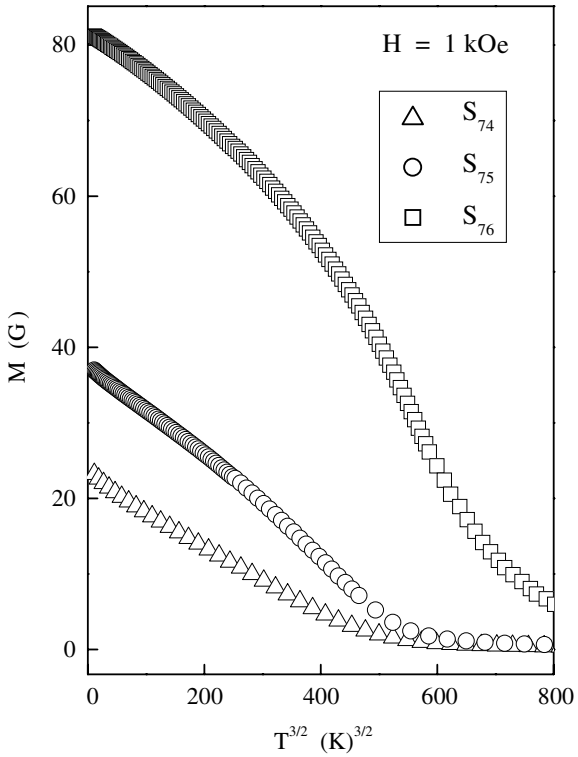

Figure 8. Magnetization measured at $H_{\rm ext} = 1$ kOe as a function of $T^{3/2}$.

$T_{\rm C}$, go smoothly to zero, in accordance with the following relations, as the concentration, p, of magnetic (Ni in the present case) atoms approaches the percolation threshold $p_{\rm c}$:

$$M(T = 0, p) = M_0(p) = m_{\rm p}(p - p_{\rm c})^{\beta_{\rm p}}[1 + a(p - p_{\rm c})^{\Delta}], \qquad p > p_{\rm c}, \quad (1)$$

$$T_{\rm C}(p) = t_{\rm p}(p - p_{\rm c})^{\phi}, \qquad p > p_{\rm c}. \quad (2)$$

In equations (1) and (2), $m_{\rm p}$ and $t_{\rm p}$ are the percolation critical amplitudes for M_0 and $T_{\rm C}$, respectively, $\beta_{\rm p}$ is the percolation critical exponent for spontaneous magnetization, ϕ is the thermal-to-percolation crossover exponent and a (Δ) is the 'correction-to-scaling' amplitude (exponent). Equations (1) and (2) are least-squares fitted to the $M_0(p)$ and $T_{\rm C}(p)$ data by treating $m_{\rm p}$, $\beta_{\rm p}$ and a ($t_{\rm p}$ and $p_{\rm c}$) as *free* fitting parameters and keeping Δ and $p_{\rm c}(\phi)$ *fixed* at $\Delta = 1$ [22–24] and in steps of 0.01 within the range $73 \leqslant p_{\rm c} \leqslant 75$, respectively (in steps of 0.01 in the range $0.3 \leqslant \phi \leqslant 0.8$). The least-squares fits to the $M_0(p)$ and $T_{\rm C}(p)$ data are depicted in figure 9 as continuous curves and the corresponding parameter values are $m_{\rm p} = 11.38(1)$, $p_{\rm c} = 73.55(5)$, $\beta_{\rm p} = 0.41(1)$, $a = 1.648(56)$, $t_{\rm p} = 46.20(8)$, $p_{\rm c} = 73.56(4)$ and $\phi = 0.50(5)$.

Aharony *et al* [25, 26] have proposed the following generalized form for the density of vibrational states of a percolating network for $p > p_{\rm C}$:

$$N(\omega) = A\omega^{x-1} f(\omega/\omega_{\rm co}) \quad (3)$$

where x represents the fracton dimensionality for which the explicit expression depends on the type of fractal model chosen, $\omega_{\rm co}$ is the frequency at which the crossover from the hydrodynamic (phonon or magnon) regime to the critical (fracton) regime takes place and A is a constant

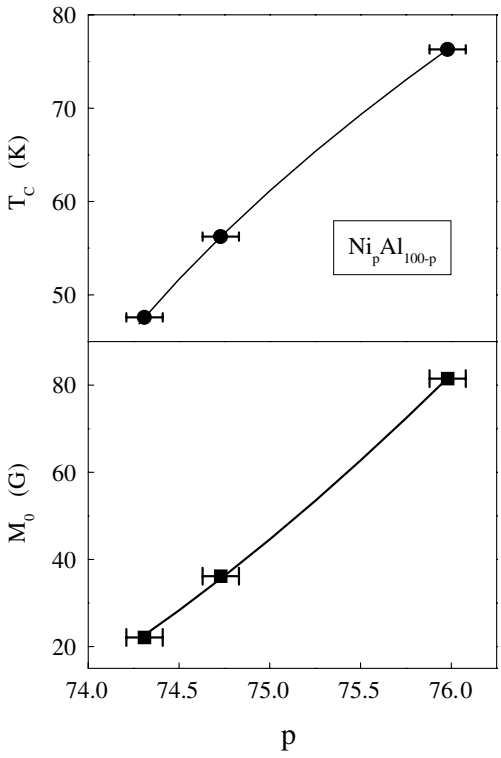

Figure 9. The spontaneous magnetization at 0 K, M_0, and the Curie temperature, T_C, as functions of Ni concentration, p.

independent of ω_{co}. $f(z)$ in the above expression is a scaling function which has the asymptotic limits $f(z) \to 1$ as $z \to \infty$ and $f(z) \to z^{d'-x}$ as $z \to 0$, so the density of vibrational states in the hydrodynamic limit ($\omega \ll \omega_{co}$) is

$$N_{hy}(\omega) = A\omega_{co}^{x-d'}\omega^{d'-1} \tag{4}$$

and in the critical limit ($\omega \gg \omega_{co}$)

$$N_{cr}(\omega) = A\omega^{x-1}. \tag{5}$$

For a phonon–fracton (magnon–fracton) crossover, the fracton dimensionality, x, and the dimension, d', are [27] $x = \tilde{d}\,(\tilde{d}_f/2)$ and $d' = d\,(d/2)$. Within the framework of this theoretical formalism, Kaul and Srinath [28] proposed the following expression for the effective density of states (DOS) in $d = 3$ percolating ferromagnetic networks:

$$n_{eff}(\omega) = (1/4\pi^2)[\hbar/D(p)]^{d/2}(p - p_c)^{\nu_p(D_f-d)}\omega^{(d/2)-1}\left(1 + \frac{\omega}{\omega_{co}}\right)^{(\tilde{d}_f-d)/2} \tag{6}$$

where $D(p)$ is the concentration-dependent spin-wave (sw) stiffness, D_f is the fractal dimension and $\tilde{d}_f$ is the ferromagnetic fracton (fr) dimensionality. *Consistent* with the asymptotic forms, equations (4)–(6) yield

$$n_{sw}(\omega) = A''\omega_{co}^{(\tilde{d}_f-d)/2}\omega^{(d/2)-1} \tag{7}$$

and

$$n_{fr}(\omega) = A''\omega^{(\tilde{d}_f/2)-1}, \tag{8}$$

with $A'' = (1/4\pi^2)\{\hbar\omega_p^{[1-(\tilde{d}_f-d)]}/d_p\}^{d/2}$, in the magnon ($\omega \ll \omega_{co}$) and fracton ($\omega \gg \omega_{co}$) regimes, respectively. Moreover, the above expression (equation (6)) for the effective DOS leads to a smooth crossover from the hydrodynamic to the critical regime at $\omega = \omega_{co}$ and gives the expected result [25–27] that the ratio $n_{fr}(\omega_{co})/n_{sw}(\omega_{co})$ is a constant *independent* of ω_{co}. In arriving at equations (7) and (8), use has been made of the expressions [25–27]

$$D_0(p) = d_p(p - p_c)^{\theta_p} \tag{9}$$

with $\theta_p = 2\nu_p[(D_f/\tilde{d}_f) - 1]$ and

$$\omega_{co} = \omega_p(p - p_c)^{2\nu_p D_f/\tilde{d}_f}. \tag{10}$$

Using the relation [27, 29]

$$D_f = d - (\beta_p/\nu_p) \tag{11}$$

and equation (1), equation (6) can be recast into the form

$$n_{eff}(\omega) = (1/4\pi^2)[\hbar/D(p)]^{d/2}[m_p^*/M_0(p)]\omega^{(d/2)-1}\left(1 + \frac{\omega}{\omega_{co}}\right)^{(\tilde{d}_f-d)/2} \tag{12}$$

where $m_p^* = m_p[1 + a(p - p_c)^{\Delta}]$.

The magnetization $M(T, H)$ is calculated by numerically integrating over the density of states, $n_{eff}(\omega)$, equation (12), using the Bose–Einstein function, which accounts for the gap introduced in the spin-wave spectrum by the *effective* field $H_{eff} = H - H_d + H_A$, where $H_d = 4\pi NM$ is the demagnetizing field and H_A is the anisotropy field (in the case where anisotropy is present), i.e.,

$$M(T, H) = M(0, H) - g\mu_B \int_0^{\omega} \frac{n_{eff}(\omega)\,d\omega}{e^{(\hbar\omega + g\mu_B H_{eff})/k_B T} - 1}. \tag{13}$$

It turns out that $M(T, H)$ is independent of the upper limit ω for $\omega > 10^{13}$ Hz. The upper limit is thus fixed at 10^{14} Hz. For a given composition and field value, the agreement between the observed and calculated values of M at different temperatures $T \leqslant T_C$ is optimized by varying $M(0, H)$, D and ω_{co}, while keeping $\tilde{d}_f$ fixed, in steps of 0.01 in the range $1.2 \leqslant \tilde{d}_f \leqslant 1.4$ in the expression for $n_{eff}(\omega)$, equation (12). It is observed that the quality of fit is improved to a great extent when the temperature dependence of the spin-wave stiffness is included in the expression for $n_{eff}(\omega)$. Among the relations

$$D(T) = D_0(1 - D_{5/2}T^{5/2}) \tag{14}$$

and

$$D(T) = D_0(1 - D_2T^2), \tag{15}$$

predicted respectively by the Heisenberg (localized-spin) and itinerant-electron models, for the temperature renormalization of the spin-wave stiffness D, the one for the itinerant case, i.e., equation (15), reproduces the $M(T, H)$ data better than that given by the Heisenberg model, as is evident from a *representative plot* of the deviations of the fits, based on equations (14) and (15), from the data, against temperature shown in figure 10. From the optimum fits based on equations (13) and (15), e.g., the continuous curves through the $M(T, H = 1$ kOe) data (symbols) shown in figure 11, the values of $D_0(p) = D(T = 0, p)$ and ω_{co} at a given field value for different compositions are obtained. It is observed that, irrespective of the field H, the power laws [22–24, 27], equations (9) and (10), are valid and describe (continuous curves in figure 12) the $D_0(p)$ and $\omega_{co}(p)$ data extremely well with the parameter values $p_c = 73.55(6)$, $\theta_p = 2\nu_p[(D_f/\tilde{d}_f) - 1] = 1.53(5)$ and $p_c = 73.53(4)$, $\theta_p + 2\nu_p = 3.25(3)$ (in $\omega_{co}(p) = \omega_p(p - p_c)^{\theta_p+2\nu_p}$, which is an alternative form of equation (10)).

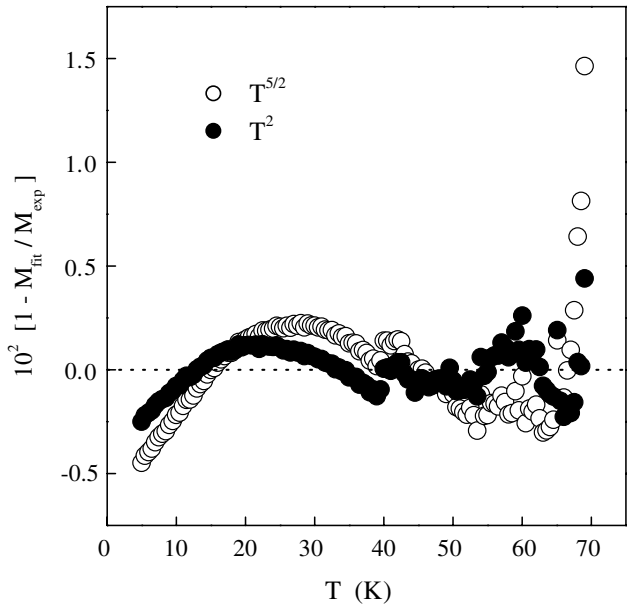

Figure 10. The percentage deviation of $M(T, H_{ext} = 1$ kOe) data from the best least-squares fits based on equations (13)–(15) for temperatures $T \leqslant T_C$.

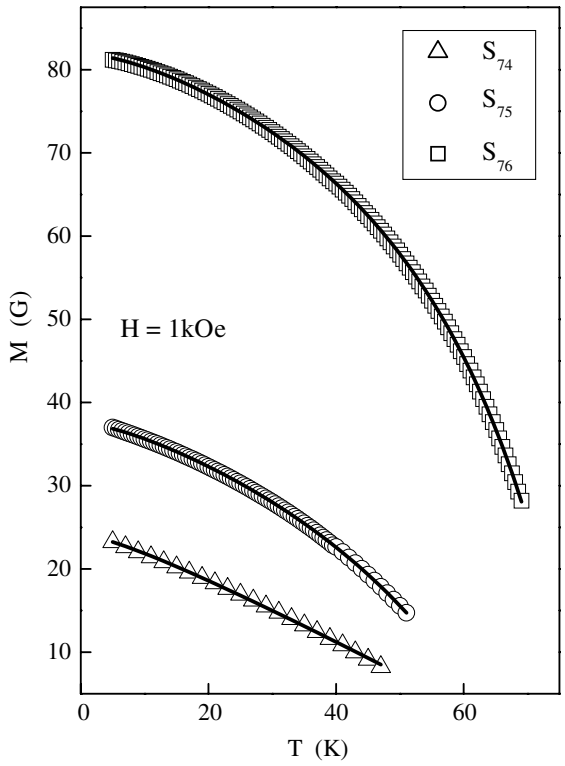

Figure 11. The temperature dependence of the magnetization at $H_{ext} = 1$ kOe for temperatures $T \leqslant T_C$. Continuous curves depict the theoretical fits based on equations (13) and (15) of the text.

With a view to emphasizing the fact that the values of exponents ϕ, θ_p, β_p along with the amplitudes t_p, d_p and m_p determined by the methods described in the preceding text are the true asymptotic values and to highlight the importance of the 'correction-to-scaling' term in the case

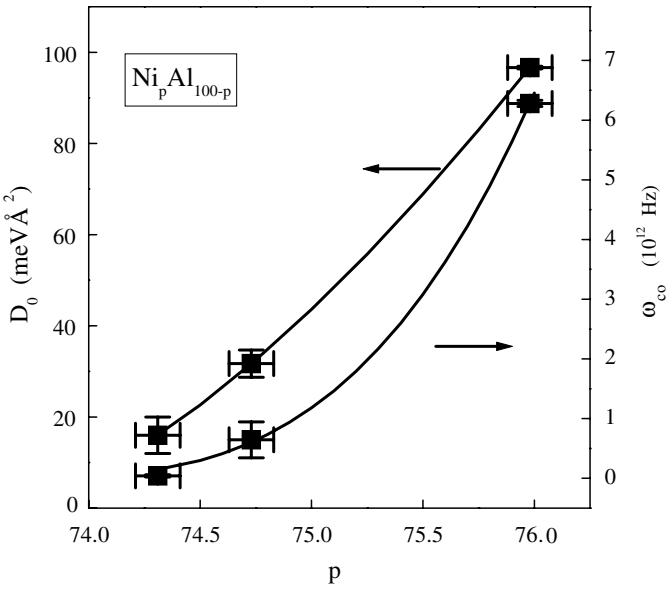

Figure 12. Variations of the spin-wave stiffness at 0 K, D_0, and the magnon-to-fracton crossover frequency, ω_{co}, with Ni concentration, p. Continuous curves depict the theoretical fits to the $D_0(p)$ and $\omega_{co}(p)$ data (solid squares) based on equations (9) and (10), respectively.

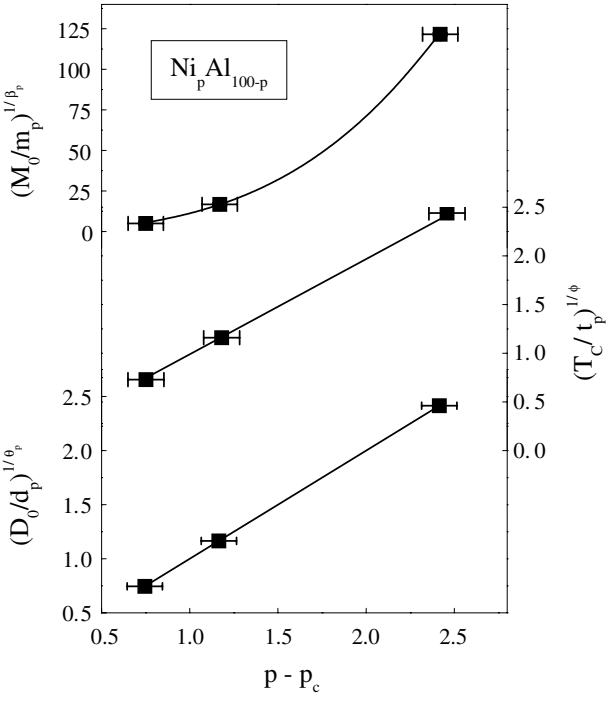

Figure 13. Variations of the quantities $(D_0/d_p)^{1/\theta_p}$, $(T_C/T_p)^{1/\phi}$ and $(M_0/m_p)^{1/\beta_p}$ with $(p - p_c)$. Continuous curves represent the theoretical fits based on equations (9), (2) and (1) of the text.

of $M(T, 0)$, the quantities $[T_C(p)/t_p]^{1/\phi}$, $[D(T = 0, p)/d_p]^{1/\theta_p}$ and $[M(T = 0, p)/m_p]^{1/\beta_p}$ are plotted against $(p - p_c)$ in figure 13. The solid straight lines and the continuous curve represent the best least-squares fits. The important observations are the following. (i) The

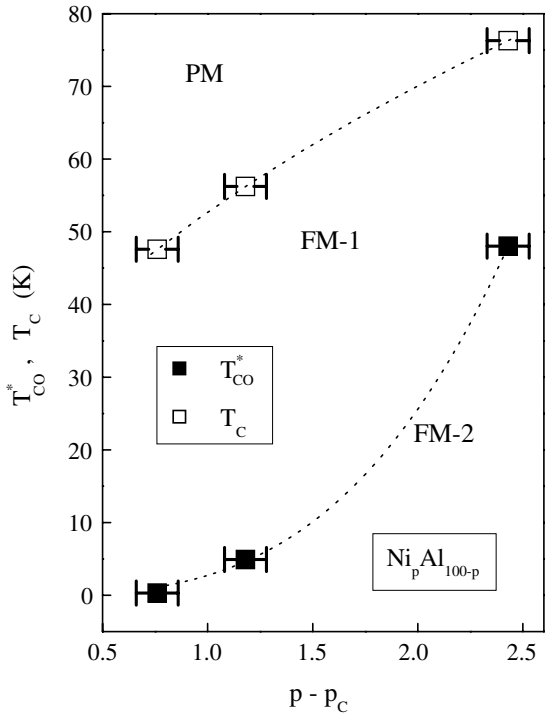

Figure 14. The magnetic phase diagram (i.e., the crossover temperatures versus the deviation of the Ni concentration, p, from the critical concentration, p_c) indicating the thermal-to-percolation (the curve, $T_C(p)$, at which the paramagnetic (PM) and ferromagnetic (FM-1) phases *coexist*) and the fracton-to-magnon (FM-1-to-FM-2), $T^*_{CO}(p)$, *crossover* lines.

$T_C(p)$, $D(T = 0, p)$ and $M(T = 0, p)$ data lead to the *same* value for p_c within the uncertainty limits for the alloy series in question. (ii) 'Correction-to-scaling' terms need to be considered in order to arrive at the true asymptotic values of β_p and m_p from the $M(T = 0, p)$ data. The values of the exponents $\theta_p + 2\nu_p$ and θ_p for $\omega_{co}(p)$ and $D_0(p)$ are used to arrive at the value for the correlation length percolation exponent $\nu_p = 0.85(4)$ whereas the relation [22–24] $\theta_p = \sigma_p - \beta_p$, where σ_p is the conductivity percolation critical exponent, defined as $\Sigma \sim (p - p_c)^{\sigma p}$, and equation (11) yield $\sigma_p = 1.94(6)$ and $D_f = 2.51(3)$. From the values of $\omega_{co}(p)$ for different concentrations, the temperature at which crossover from the hydrodynamic (magnon) regime to the critical (fracton) regime occurs [29], $T^*_{co}(p) = \hbar\omega_{co}(p)/k_B$, has been evaluated. The $T^*_{co}(p)$ curve represents the crossover line that divides the ordered (*ferromagnetic*, FM) phase into two (FM-2, *hydrodynamic* and FM-1, *critical*) regions in the magnetic phase diagram (figure 14) in the lower-temperature regime. This line is in addition to the thermal-to-percolation crossover line, $T_C(p)$, that establishes the boundary between the ordered (FM) and disordered (*paramagnetic*, PM) magnetic phases in figure 14.

The values of percolation exponents θ_p, β_p, ν_p, σ_p, their ratios β_p/ν_p, σ_p/ν_p, the thermal-to-percolation crossover exponent ϕ, the fractal dimension D_f and the ferromagnetic fracton dimensionality $\tilde{d}_f$ yielded by the above-mentioned data analysis are tabulated and compared with the corresponding theoretical estimates [22–24, 27] for percolation on a *regular* $d = 3$ lattice in table 3. A very good agreement between the experimentally determined and theoretically predicted values (except for the crossover exponent ϕ), as evidenced from

Table 3. Comparison between experiment and theory.

Parameter	Experiment	Theory [22–24, 27]
ϕ	0.50(5)	1.10(2)
θ_p	1.53(5)	1.52(3)
β_p	0.41(1)	0.41(1)
ν_p	0.85(4)	0.87(7)
σ_p	1.94(6)	2.00(5)
β_p/ν_p	0.48(3)	0.471(16)
σ_p/ν_p	2.28(6)	2.31(6)
D_f	2.51(3)	2.50(2)
$\tilde{d}_f$	1.32(3)	4/3

the entries in table 3, strongly indicates that the percolation picture is applicable to the alloys in question. Similar agreement between experiment and theory has been previously observed [28, 30] in several quenched random site-diluted ferromagnetic systems (dilute magnetic amorphous alloys). An obvious deduction from this agreement is that quenched randomness does not alter the critical behaviour of percolation on a regular $d = 3$ lattice. While the result $\tilde{d}_f = 1.32(3)$ vindicates the Alexander–Orbach conjecture [31] (which states that the fracton dimensionality $\tilde{d}_f = 4/3$ for percolating networks with Euclidean dimension $d \geqslant 2$) for $d = 3$, the finding that $\sigma_p = 1.94(6)$ is consistent with the Golden inequality [32] $\sigma_p \leqslant 2$ for $d = 3$.

The results yielded by the analysis based on percolation ideas raise the following pertinent questions.

(1) How reliable are the exponent values with *just three* data points corresponding to the three compositions studied?
(2) How can one justify using a percolation (localized-spin) approach to describe weak *itinerant-electron* ferromagnets?

Despite scanty data, a high level of confidence in the exponent values quoted in table 3 is justified on two counts. First, considering that an accurate estimate of the percolation threshold p_c is absolutely crucial to the determination of the percolation exponents, the different data sets $T_C(p)$, $M_0(p)$, $D_0(p)$, $\omega_{co}(p)$ and $\mathcal{S}^{-1}(p)$ yield the *same* value for p_c within the uncertainty limits. Second, in the alloy with composition ($Ni_{73.52}Al_{26.48}$) very close to $p_c = 73.55$ at.% Ni, no long-range ferromagnetic order has been observed for temperatures down to 5 K. However, a large number of data points are certainly needed to refine the value of p_c and hence to determine the exponents with much greater accuracy. The *fractal* nature of the magnetic network in the *site-disordered* Ni_pAl_{100-p} alloys with p near p_c could be the result of the high degree of quenched random disorder and/or chemical inhomogeneity (as inferred from the x-ray diffraction patterns shown in figure 1). Thus, even though the samples in question exhibit weak itinerant-electron ferromagnetism, the percolation behaviour can be attributed to the random-disorder-induced localization of magnetic moments. For dilute ferromagnets with composition (p) in close proximity to the percolation threshold (p_c), *finite* magnetic clusters with a broad size distribution coexist [33] with an *infinite* ferromagnetic network. As the concentration of magnetic atoms, p, is increased above the percolation threshold, p_c, the infinite ferromagnetic network grows at the expense of finite ferromagnetic clusters whose number reduces [33] rapidly and the size distribution narrows down [34]. Indirect experimental evidence for the existence of such finite ferromagnetic clusters at temperatures above T_C comes from the concave-downward curvature in the M versus H isotherms and the deviations from the Curie–

Weiss law behaviour of magnetic susceptibility that persist to temperatures as high as $\sim 2T_C$ ($\sim 6T_C$) for the 'as-prepared' and 'annealed' samples ('quenched sample') of $Ni_{75}Al_{25}$ [10, 17].

At this stage, it is worth noting that the magnetic parameters for the 'quenched' sample S_2 of paper I do not follow the variations with Ni concentration observed for the samples S_{74}, S_{75} and S_{76} (figures 4, 5, 9 and 12) even though the long-range order parameter **S** has the same value for S_2, S_{74}, S_{75} and S_{76} within the uncertainty limits. This is so because the sample S_2, unlike the samples S_{74}, S_{75} and S_{76}, has a very high concentration of vacancies (point defects) which, in turn, accounts for a significant part of site disorder in this sample (for details, refer to section 3 of paper I).

Finally, D_0 is plotted against M_0 in figure 7 with a view to ascertaining whether the compositional disorder affects the band parameter $c_\perp$ in the relation $D_0 = g\mu_B c_\perp M_0$, predicted by the spin fluctuation models [19, 20]. Consistent with the previous inferences, a nonlinear variation of D_0 with M_0 implies that the compositional disorder does affect the shape of the DOS curve near E_F.

4. Conclusion

The results of the present investigation reveal that the compositional disorder has a profound effect on the magnetic properties of *site-disordered* Ni_pAl_{100-p} alloys, as elucidated below.

Like site disorder, compositional disorder smears out the sharp features in the density of states (DOS) curve near the Fermi level, E_F, and reduces the DOS at E_F, $N(E_F)$, with the result that a sizable reduction (increase) occurs in the spontaneous magnetization at 0 K, M_0, the spin-wave stiffness at 0 K, D_0, and the Curie temperature, T_C (zero-field differential susceptibility at 0 K, χ_0). In sharp contrast with the *abrupt* variations in the physical quantities caused by site disorder, $N(E_F)$ (and hence the inverse Stoner enhancement factor $\mathcal{S}^{-1} = IN(E_F) - 1$), M_0, D_0, T_C and even the D_0/T_C ratio (χ_0) *decrease* (*increase*) *smoothly* with increasing compositional disorder brought about by lowering the Ni concentration (p) towards the *critical value* (p_c) at which the long-range ferromagnetic order disappears. The functional dependences of M_0, D_0 and T_C on p are very well described by the *power laws* $M_0(p) \sim (p - p_c)^{\beta_p}$, $D_0(p) \sim (p - p_c)^{\theta_p}$ and $T_C(p) \sim (p - p_c)^{\phi}$ with $p > p_c$, which, according to the percolation theories, characterize the percolation critical behaviour (second-order phase transition) at $p = p_c$ in three-dimensional ($d = 3$) ferromagnetic percolating networks. The other important finding is that a crossover in the spin dynamics from the hydrodynamic (*magnon*) to critical (*fracton*) regime occurs at a well-defined temperature $T^*_{co}(p)$. The present results, in addition: (i) permit a reasonably accurate determination of the hydrodynamic-to-critical spin-wave crossover line in the magnetic phase diagram, the percolation-to-thermal crossover exponent, fractal dimension, fracton dimensionality, the percolation critical exponents for spontaneous magnetization, spin-wave stiffness, correlation length and conductivity; and (ii) vindicate the Alexander–Orbach conjecture and the Golden inequality for $d = 3$ percolating ferromagnetic networks.

Acknowledgment

This work was supported by the Department of Science and Technology, India, under the grant DO No SP/S2/M-21/97.

References

[1] Massalski T B (ed) 1990 *Binary Alloy Phase Diagrams* vol 1 (Metals Park, OH: ASM International)
[2] de Boer F R, Schinkel C J, Biesterbos J and Proost S 1969 *J. Appl. Phys.* **40** 1049

[3] de Chatel P F and de Boer F R 1970 *Physica* **48** 331
[4] Hambourger P D, Olwert R J and Chu C W 1975 *Phys. Rev.* B **11** 3501
[5] Buis N, Franse J J M and Brommer P E 1981 *Physica* B **106** 1
[6] Sasakura H, Suzuki K and Masuda Y 1984 *J. Phys. Soc. Japan* **53** 754
[7] Suzuki K and Masuda Y 1985 *J. Phys. Soc. Japan* **54** 630
[8] Dhar S K, Gschneidner K A Jr, Miller L L and Johnston D C 1989 *Phys. Rev.* B **40** 11488
[9] Yoshizawa M, Hirotaka S, Ikeda K, Okuno K, Saito M and Shigematsu K 1992 *J. Phys. Soc. Japan* **61** 3313
[10] Semwal A and Kaul S N 2004 Magnetic properties of the weak itinerant-electron ferromagnet $Ni_{75}Al_{25}$: I. *J. Phys.: Condens. Matter* **16** 8675
[11] Stoner E C 1939 *Proc. R. Soc.* A **139** 339
[12] Wohlfarth E P 1953 *Rev. Mod. Phys.* **25** 211
[13] Moriya T and Kawabata A 1973 *J. Phys. Soc. Japan* **34** 639
Moriya T and Kawabata A 1973 *J. Phys. Soc. Japan* **35** 669
[14] Bernhoeft N R, Cole I, Lonzarich G G and Squires G L 1982 *J. Appl. Phys.* **53** 8204
[15] Bernhoeft N R, Lonzarich G G, Mitchell P W and Paul D McK 1983 *Phys. Rev.* B **28** 422
[16] Semwal A and Kaul S N 1999 *Phys. Rev.* B **60** 12799
[17] Semwal A and Kaul S N 2002 *J. Phys.: Condens. Matter* **14** 5829
[18] Aoki K and Izumi O 1975 *Phys. Status Solidi* **32** 657
[19] Lonzarich G G and Taillefer L 1985 *J. Phys. C: Solid State* **18** 4339
[20] Kaul S N 1999 *J. Phys.: Condens. Matter* **11** 7597
[21] Buis N, Franse J J M and Broumer P E 1981 *Physica* B **106** 1
[22] Kirkpatrick S 1972 *Rev. Mod. Phys.* **45** 574
[23] Essam J W 1980 *Rep. Prog. Phys.* **43** 833
[24] Stauffer D and Aharony A 1991 *Introduction to Percolation Theory* (Bristol: Taylor and Francis)
[25] Aharony A, Alexander S, Entin-Wohlman O and Orbach R 1985 *Phys. Rev.* B **31** 2565
[26] Aharony A, Entin-Wohlman O, Alexander S and Orbach R 1987 *Phil. Mag.* B **56** 949
[27] Nakayama T, Yakubo K and Orbach R 1994 *Rev. Mod. Phys.* **66** 381 and references cited therein
[28] Kaul S N and Srinath S 2001 *Phys. Rev.* B **63** 094410
[29] Stinchcombe R B and Pimentel I R 1988 *J. Phys. A: Math. Gen.* **21** L807
[30] Kaul S N and Babu P D 1994 *Phys. Rev.* B **50** 9323
[31] Alexander S and Orbach R 1982 *J. Physique* **43** L625
[32] Golden K 1990 *Phys. Rev. Lett.* **65** 2923
[33] Kaul S N 1980 *Solid State Commun.* **36** 279
Kaul S N 1984 *IEEE Trans. Magn.* **20** 1290
Kaul S N 1985 *J. Magn. Magn. Mater.* **53** 5
[34] Kaul S N 1991 *J. Phys.: Condens. Matter* **3** 4027
Kaul S N, Siruguri V and Chandra G 1992 *Phys. Rev.* B **45** 12343
Kaul S N and Babu P D 1998 *J. Phys.: Condens. Matter* **10** 1563